# Phased Array Calibration Based on Measured Complex Signals in a Compact Multi-probe Setup

Zhang, Yusheng; Wang, Zhengpeng ; Zhang, Fengchun; Chen, Xiaoming ; Miao, Jungang ; Fan, Wei

*Published in:*
I E E E Antennas and Wireless Propagation Letters

*DOI (link to publication from Publisher):*
10.1109/LAWP.2022.3149966

*Publication date:*
2022

*Document Version*
Accepted author manuscript, peer reviewed version

# Phased Array Calibration Based on Measured Complex Signals in a Compact Multi-probe Setup

Yusheng Zhang, Zhengpeng Wang, Fengchun Zhang, Xiaoming Chen, Jungang Miao, Wei Fan

***Abstract*—Phased array calibration is typically carried out in plane-wave conditions, which requires expensive far-field setups. This letter presents a novel phased array calibration method based on measured complex array signal, which works in the cost-effective compact testing setup. The basic principle is to employ multi-probe antennas in a short measurement distance such that we can effectively retrieve the array element patterns in the boresight direction based on the recorded complex signals at the multiple probes using the interpolation technique. Both theoretical derivations and measurement validations are provided to demonstrate the effectiveness of the proposed method.**

***Index Terms*—Over-the-air testing, phased array, array calibration**

## I. Introduction

Phased arrays have been extensively employed in various communication and radar applications, due to their capabilities, e.g. to electronically form beams or nulls in different directions. Phased array calibration is essential to ensure phased array performance, where the objective is to detect and compensate out the imhomegenities (i.e. complex excitations) among phased array elements [1].

Various array calibration methods have been reported in the literature [1]–[6]. One cost-effective strategy is to measure the response of each array element sequentially with only one element activated and other elements properly terminated (i.e. on-off mode) [6]. The measurement can be carried out with the help of a near-field scanner and a probe antenna aligned with the illuminated array element (i.e. face-to-face). However, the near-field setup requires high repositioning precision of the near field scanner system, precise knowledge of the phased array antenna configuration and dedicated effort to align the near field scanner and the antenna under test (AUT) [7].

Alternatively, the far-field setup with a single probe antenna located in the bore-sight of the phased array can be employed. However, as antenna systems increase in size and operating frequency, it becomes increasingly difficult to meet the Fraunhofer distance requirement in the direct far-field setups. Another drawback with the direct far-field setup is the reduced dynamic range, which is important for accurate measurements. Indirect far-field setups, i.e. the compact antenna test range (CATR) and the plane wave generator (PWG), have been widely reported [8], [9]. Both methods can physically generate a uniform plane wave with a much reduced measurement distance. However, both the reflector in the CATR setup and the PWG array require careful design, manufacturing and maintenance. In the far-field setup, phased array calibration can be carried out in two modes, i.e. on-off mode and all-on mode (i.e. with all elements activated). Various phase toggling algorithms have been proposed in the all-on mode. An inverse method was proposed in [10], and multi-probe measurement setup was introduced to improve the conditioning of system. A recursive matrix-forming method was proposed in [2], which can be used to generate well-conditioned excitation matrix. The method was further improved in [4], where the accumulated error at the first array element can be effectively removed. In [3], an algorithm was proposed to calibrate phased array working in the default beamforming mode. However, the algorithm only works when the beam-steering interval is large. To address this problem, a multi-probe strategy is proposed in [5] to virtually increase beam angular interval steered by the AUT array, thus improving the calibration accuracy.

However, to the best knowledge of the authors, far-field setups are generally required for the discussed algorithms [1]–[6]. In this work, we propose to calibrate the phased array antenna systems in a compact multi-probe setup. The proposed algorithm is valuable, especially for large-aperture AUTs whose far-field condition cannot be met. The basic idea is to employ multiple probe antennas to measure the far-field radiation pattern samples of the AUT elements and then interpolating the far-field pattern samples to obtain the far-field patterns of the AUT elements, and finally the reconstructed far-field pattern in the boresight direction of each AUT element can be extracted for array calibration.

We discuss the signal model and the state-of-the-art methods in Section II. The proposed method is described in Section III. The validation measurement is presented in Section IV, and Section V concludes the work.

## II. Signal model and the state-of-the-art methods

### A. Signal Model

The compact multi-probe measurement system is illustrated in Fig. 1. The feed of the AUT is split into $N$ branches, each connected to a phase shifter, an attenuator and an AUT element in the RF chain. $P$ sets of complex weights can be assigned to the AUT elements. For array calibration purpose, individual phase tuning and attenuation control per element might be required [1], [2], [6]. $M$ probe antennas are placed in an anechoic chamber, as illustrated in Fig. 1. Our discussion is limited to the single polarized case, though its extension to dual-polarized case is straightforward.

Yusheng Zhang, Zhengpeng Wang and Jungang Miao are Electronics and Information Engineering, Beihang University, Beijing 100191, China

Fengchun Zhang and Wei Fan are with the Antenna Propagation and Millimeter-wave Systems (APMS) section, Aalborg University, Denmark.

Xiaoming Chen is with School of Information and Communications, Xi'an Jiaotong University, Xi'an 710049, China

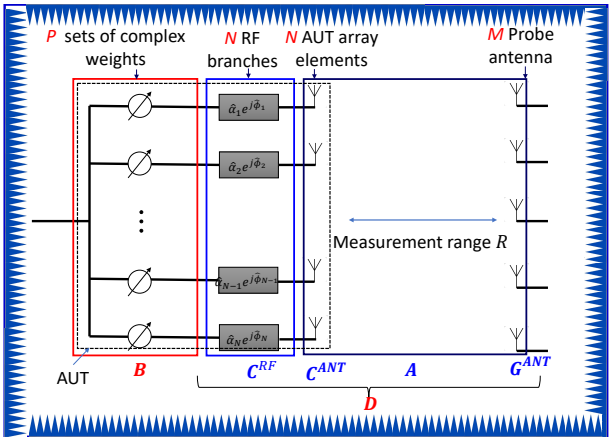


Figure 1. System diagram for the measurement system.

As explained, we need to determine inhomogeneities among signal paths in the AUT. In over-the-air (OTA) measurements, radio waves are used to connect AUT to probe antenna and test instrument. Therefore, AUT element pattern becomes a non-separable part of the signal path. We denote the signal path vector to be determined as $\boldsymbol{h}^{RF} \in \mathbb{C}^{N\times 1}$, with its $n$-th element $h_n^{RF}$ defined as:

$$h_n^{RF} = \alpha_n \exp^{j\phi_n} = \hat{\alpha}_n \exp^{j\hat{\phi}_n} c_n^o, \tag{1}$$

where $\hat{\alpha}_n$ and $\hat{\phi}_n$ denote the amplitude and phase term in the $n$-th RF chain and $c_n^o$ denotes the complex antenna pattern of the $n$-th AUT element in the boresight direction, respectively. $\alpha_n$ and $\phi_n$ denote the initial amplitude and phase terms to be determined in the $n$-th signal path, respectively.

The signal model of the multi-probe measurement system can be written in general as:

$$\boldsymbol{S} = \boldsymbol{B} \cdot \boldsymbol{D}, \tag{2}$$

where the excitation matrix $\boldsymbol{B} \in \mathbb{C}^{P\times N}$, and transfer matrix $\boldsymbol{D} \in \mathbb{C}^{N\times M}$ characterize two sub-parts of s-parameter matrix $\boldsymbol{S} \in \mathbb{C}^{P\times M}$, respectively, as detailed below:

- $\boldsymbol{S} = \{s_{pm}\}$ is the complex s-parameter matrix between the AUT antenna feed and $M$ probe antenna feeds for $P$ sets of complex weights. The complex vector $\boldsymbol{S}$ can be directly measured, e.g. via a vector network analyzer (VNA). Note that $P \geq N$ is required to solve (2).
- $\boldsymbol{B} = \{b_{pn}\}$, with $b_{pn}$ being the complex weight applied to the $n$-th AUT element for the $p$-th set of weights.
- $\boldsymbol{D} = \{d_{nm}\}$ is the transfer matrix, which is given as:

$$\boldsymbol{D} = (\boldsymbol{C}^{RF} \cdot \boldsymbol{C}^{ANT}) \odot \boldsymbol{A} \odot \boldsymbol{G}^{ANT}, \tag{3}$$

where $\odot$ denotes the Hadamard (i.e. element-wise) product. The components of $\boldsymbol{D}$ are explained below.

  - $\boldsymbol{C}^{RF} \in \mathbb{C}^{N\times N}$ is an RF response matrix to denote the inhomogeneities among RF chains (excluding AUT antenna element pattern). It is a diagonal matrix with its diagonal element $c_n^{RF} = \hat{\alpha}_n \exp^{j\hat{\phi}_n}$.
  - $\boldsymbol{C}^{ANT} \in \mathbb{C}^{N\times M}$ is the AUT antenna pattern matrix, with its element $c_{nm}^{ANT}$ denoting the complex antenna pattern of the $n$-th AUT element at the $m$-th probe antenna direction. $\boldsymbol{C}^{ANT}$ is typically unknown, which makes it difficult to determine $\boldsymbol{h}^{RF}$.
  - $\boldsymbol{A} \in \mathbb{C}^{N\times M}$ is the free space transfer function matrix. $\boldsymbol{A}$ can be calculated, once the probe locations and AUT element locations are accurately known.
  - $\boldsymbol{G}^{ANT} \in \mathbb{C}^{N\times M}$ is the probe pattern matrix, with the entry $g_{nm}^{ANT}$ denoting the radiation pattern of the $m$-th probe antenna in the $n$-th AUT element direction. $\boldsymbol{G}^{ANT}$ can be measured in advance.

### B. Single Probe Antenna methods

*1) On-off mode :* In the on-off mode, we basically enable the $n$-th signal path and disable all the other $N-1$ signal paths, for $n \in [1, N]$. $\boldsymbol{B} = \boldsymbol{I}_N$ is effectively set with $P = N$ in the on-off mode, with $\boldsymbol{I}_N$ the identity matrix. As discussed, with a single probe antenna (i.e. with $M = 1$) located in the boresight of the AUT, (2) and (3) can be simplified as:

$$\begin{aligned}\boldsymbol{s} =& \boldsymbol{B} \cdot \boldsymbol{h}^{RF} \cdot \left[c_{11}^{ANT}/c_1^o, ..., c_{N1}^{ANT}/c_N^o\right]^T \\ & \odot \left[a_{11}, ..., a_{N1}\right]^T \odot \left[g_{11}^{ANT}, ..., g_{N1}^{ANT}\right]^T,\end{aligned} \tag{4}$$

where vector $\boldsymbol{s} \in \mathbb{C}^{N\times 1}$, $\left[a_{11}, ..., a_{N1}\right]^T \in \mathbb{C}^{N\times 1}$ and $\left[g_{11}^{ANT}, ..., g_{N1}^{ANT}\right]^T \in \mathbb{C}^{N\times 1}$ correspond to matrix $\boldsymbol{S}$, $\boldsymbol{A}$ and $\boldsymbol{G}^{ANT}$ with $M = 1$ set, respectively. $[]^T$ denotes the transpose operator. As we can see, $\boldsymbol{h}^{RF}$ cannot be determined unless $c_{n1}^{ANT}/c_n^o$ is known for $n \in [1, N]$. However, AUT antenna pattern matrix $\boldsymbol{C}^{ANT} \in \mathbb{C}^{N\times M}$ is typically not known. When the probe antenna is placed in the boresight direction of the AUT under the far-field condition, we have $c_{n1}^{ANT}/c_n^o = 1$ and $g_{n1}^{ANT} = g^{ANT}$ for $n \in [1, N]$. Vector $\left[a_{11}, ..., a_{N1}\right]^T$ can be calculated based on free-space propagation coefficient. $\boldsymbol{h}^{RF}$ can be therefore directly solved in (4) in $N$ on-off measurements (i.e. with $\boldsymbol{B} = \boldsymbol{I}_N$). Note that when the measurement distance is smaller than the Fraunhofer distance of the AUT, the signal path $h_n^{RF}$ will be distorted by the unknown AUT element pattern term $c_{n1}^{ANT}/c_n^o$, which is the problem we aim to solve in this work.

*2) All-on mode :* With the probe located in the far-field, we can obtain $\boldsymbol{h}^{RF}$ via solving linear equations as.

$$\boldsymbol{h}^{RF} \odot \left[a_{11}, \cdots, a_{N1}\right]^T = \boldsymbol{B}^+ \cdot \boldsymbol{s}, \tag{5}$$

where $()^+$ is the pseudo-inverse operator. In practice, there exists perturbation in both $\boldsymbol{B}$ and $\boldsymbol{s}$. Condition number of matrix $\boldsymbol{B}$, measures the sensitivity of the solution to the perturbation. For an ill-conditioned matrix $\boldsymbol{B}$, even a small perturbation would lead to a significant change in $\boldsymbol{h}^{RF}$, making it unfeasible to obtain accurate array calibration in practice. Many works have been reported to design well-conditioned $\boldsymbol{B}$ [2]–[5]. Similar to the on-off mode, we can obtain accurate array calibration results, only when the probe antenna is placed in the far-field region of the AUT.

## III. Proposed Compact Multi-Probe Method

### A. Principle

As discussed, the main problem is that $h_n^{RF}$ will be distorted by the unknown AUT element pattern term $c_{n1}^{ANT}/c_n^o$ in the

single probe near-field setup. The main contribution of this work is that we propose to employ interpolation strategy to obtain the unknown AUT element patterns in the boresight direction in the compact multi-probe setup, thus enabling phased array calibration with short measurement distance.

Based on (2) and (3), the known free-space propagation matrix $\boldsymbol{A}$ and probe antenna matrix $\boldsymbol{G}^{ANT}$ can be compensated:

$$\boldsymbol{C}^{RF} \cdot \boldsymbol{C}^{ANT} = (\boldsymbol{B}^{+} \cdot \boldsymbol{S}) \oslash \boldsymbol{A} \oslash \boldsymbol{G}^{ANT} = \boldsymbol{F}, \qquad (6)$$

where $\oslash$ denotes the element-wise matrix division. $\boldsymbol{F} = \{f_{nm}\} \in \mathbb{C}^{N \times M}$ is defined as in (6) for notation simplicity. With $M$ probe antennas in the setup, we have $M$ pattern samples for each AUT element antenna in the $M$ probe antenna directions in principle. We can reconstruct the boresight direction pattern of the $n$-th AUT element based on the $M$ measured pattern samples, i.e. $c_{nm}^{ANT}$ for $m \in [1, M]$, via an interpolation process. Our objective is to reconstruct the radiation pattern in the boresight direction of each AUT element based on the $M$ samples measured by the probes.

Applying the interpolation technique, (6) can be written as:

$$\begin{aligned} \hat{\boldsymbol{h}}^{RF} &= \boldsymbol{C}^{RF} \cdot [\hat{c}_1^o, ..., \hat{c}_n^o, ..., \hat{c}_N^o]^T \\ &= [\hat{f}_1(\theta_o), ..., \hat{f}_n(\theta_o), ..., \hat{f}_N(\theta_o)]^T, \end{aligned} \qquad (7)$$

where $\hat{f}_n(\theta_o)$ is the interpolated complex coefficient for the $n$-th AUT element in the boresight direction based on $\boldsymbol{F}$.

### B. Discussion

In the measurement setup, multiple probes should be placed in the near-field region of the AUT (array) while in the far-field region of the AUT elements, as illustrated in Fig. 2, where $R_{min}$ represents the minimal measurement distance required by the far-field distance of the AUT element and the probe antennas, which is much smaller than that of the whole AUT array. In addition, the $M$ probes antennas should be distributed in a large enough angular region to at least cover all the boresight directions of the AUT elements to avoid extrapolation issue, which will result in a large reconstruction error of the far-field pattern of the AUT elements. In principle, the number of required probes $M$ should be no larger than $N$. When $N$ probe antennas are aligned face-to-face with each individual AUT element, the boresight direction pattern of each AUT element can be directly obtained without pattern interpolation. Below we discuss how to derive the minimal number of probes for a specific multi-probe setup.

For a linear AUT with a given aperture $L$ and at a given measurement distance $R$ as illustrated in Fig. 2, two probe antennas are firstly located aligning face-to-face with the AUT elements at the two ends and the rest $M-2$ probe antennas are uniformly placed in between. The maximum angular sampling interval (ASI) of the pattern samples recorded by the $M$ probes for AUT elements is denoted by $\theta_{max}$, which can be given as:

$$\theta_{max} = 2\tan^{-1}\left[\frac{L}{2R(M-1)}\right]. \qquad (8)$$

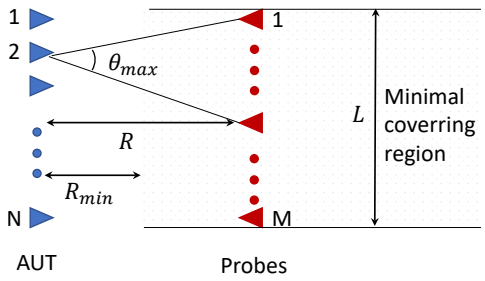


Figure 2. An illustration of probe location design principle.

As discussed in [11], the more radiation pattern samples we have, a better reconstructed pattern can be achieved via interpolation for a given antenna. The reference [11] also concluded that more radiation pattern samples (with a smaller ASI) are required for a more directional antenna (i.e. with a narrower half-power beam width (HPBW)) and the HPBW of the antenna is the maximum ASI setting to achieve a good main beam pattern reconstruction via interpolating limited pattern samples. In our method, we recommend that $\theta_{max} = \Omega_{3dB}/2$ with $\Omega_{3dB}$ denoting the HPBW of the AUT elements. Thus, the minimum $M$ can be calculated according to (8):

$$M_{min} = \min\left\{\left\lceil \frac{L}{2R\tan(\frac{\Omega_{3dB}}{4})} + 1 \right\rceil, N\right\}, \qquad (9)$$

where $\lceil \cdot \rceil$ denotes the rounding up operator. The equation shows that the minimum probe number $M$ increases as the measurement distance $R$ normalized by the AUT aperture $L$ and the HPBW $\Omega_{3dB}$ of the AUT elements decrease. Note that array element pattern is typically not directional to enable a large beam scanning range. Therefore, a few probe antennas should be sufficient for AUT element pattern interpolation.

## IV. Validation Measurements

### A. Measurement System

The experimental system, as illustrated in Fig. 3, consists of 1) a uniform linear array (ULA) served as the AUT composed of 14 single-polarized waveguide antenna elements with a spacing of 86.5mm, where the AUT is selected from a 2D planar array as shown in Fig. 3; 2) an 14-port phase control network composed of a power spliter, 8-bit programmable phase shifters with a tuning range of $[0^o, 360^o)$ and step resolution of $1^o$; 3) the multi-probe system, realized by moving a single probe to preset locations with the help of a scanner. Two probe systems were employed in the measurements. In the first system, one WR284 waveguide probe antenna with 5.6 dBi gain at 2.6 GHz and HPBW of $127^o$ was employed for $R = 0.5$ m distance. In the second system, one standard gain horn antenna with 10.4 dBi gain at 2.6 GHz and HPBW of $57.8^o$ was used for $R = 1$ m distance. For each system, the probe is moved to 7 locations with a spacing of 0.187 m and 5 locations with a spacing of 0.281 m, respectively; 4) a VNA to generate the signal fed to the AUT and to record the signals received at the multiple probe locations; 5) a low-noise amplifier operating at 1-12 GHz with a typical gain 35

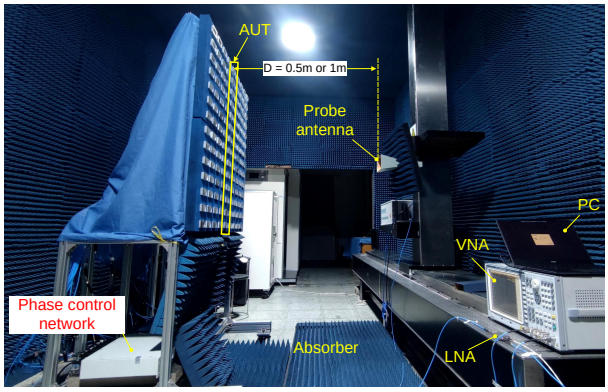


Figure 3. A photo of the measurement setup.

dB. Note that pyramid absorbers are used to cover the AUT array, the bottom of the AUT array and the ground to minimize potential reflections. In the measurement, the single tone signal at 2.6 GHz generated by the VNA is fed into the power splitter, weighted by the complex weights realized by the phase control network, and then radiated by the AUT. The complex signals received by the probe antenna at the multiple locations are then recorded by the VNA.

### B. Measurement Campaign

Two measurement campaigns were conducted to validate the proposed method. 1) In the reference measurement campaign, we directly measure the calibration coefficients of AUT elements via the element far-field on-off measurement. A waveguide antenna, same as the one employed for the AUT array elements, is used as the probe antenna, which is carefully aligned with each AUT element "face-to-face" with a distance of 0.5 m. The amplitude is set to 0 dB for the aligned AUT element and $-120$ dB for other AUT elements while the phases are set to $0^o$ for all AUT elements. Note that the AUT element far-field distance is 0.112 m at 2.6 GHz. 2) In the validation measurement campaign, we obtain the calibration coefficients with the proposed compact multi-probe setups via employing the aforementioned two probe systems. Basically, for each probe location, we set the excitation matrix $\boldsymbol{B}$ according to the Hadamard matrix of order 16 [2], [4] and recorded the complex signals for each phase shifter settings of the AUT elements, where the 1st and 2nd elements are assumed dummy elements. The amplitude excitations are fixed to 0 dB, while the phase excitations are set to $0^o$ and $180^o$, depending on the Hadamard matrix structure. We then repeat the same measurements for the other locations. As discussed, a 7-probe configuration and a 5-probe configuration are employed for both measurement distances. Therefore, we have 384 complex signal measurements in total. We can then retrieve the AUT array initial excitations based on Eq. (6) and Eq. (7). Note that the measurement results for 4-probe, 3-probe and 1-probe configurations can be extracted based on the measurement data of the 7-probe configuration.

Table I
CALIBRATION ERROR DYNAMIC RANGE FOR THE VARIOUS MEASUREMENT SETTINGS.

| M | Amp error [dB] @ 0.5m / @1m | Phase error [deg] @ 0.5m / @1m |
|---|---|---|
| 7 | 0.9 / 0.8 | 4.0 / 4.7 |
| 5 | 1.0 / 0.7 | 6.6 / 12.0 |
| 4 | 0.8 / 1.0 | 7.5 / 5.6 |
| 3 | 1.8 / 1.0 | 19.1 / 6.7 |
| 1 | 2.5 / 2.4 | 53.7 / 32 |

### C. Measurement Results

The calibration errors for various settings, i.e., different probe antennas, measurement distances and probe configurations, are summarized in Table I. We can see that:

- For a given measurement distance, the calibration error increases as the probe number $M$ decreases, due to the enlarged interpolation errors introduced by the larger ASI of the measured pattern samples, where fewer pattern samples are measured within a given angular range.
- For a given number of probes, the calibration error increases as the measurement distance decreases, due to the enlarged interpolation errors introduced by the increased ASI of the measured pattern samples, where a larger angular region is covered by a fixed number of pattern samples.
- According to (9), $M_{min} = 5$ and $M_{min} = 3$ are the minimum required number of probes for the measurement distances $R = 0.5$ m and $R = 1$ m, respectively, where a calibration error up to $\pm 0.5$ dB in amplitude and $\pm 3.4^o$ in phase can be achieved.

According to the specification of the phase shifter, an amplitude uncertainty of $\pm 0.5$ dB and a phase uncertainty of $\pm 5^o$ might be expected for each phase state.

## V. CONCLUSION

Phased array calibration is typically carried out in the single probe antenna far-field setup. It is desirable that the phased array calibration can be done with much reduced measurement distance. Therefore, a novel phased calibration method by employing multi-probe antennas is proposed in this work. The main contribution of this work is to employ interpolation strategy to obtain the unknown AUT element patterns in the boresight direction in the compact multi-probe setup, thus enabling phased array calibration with a short measurement distance. The measurement results demonstrate the effectiveness and robustness of the proposed method. Good calibration results can be achieved with 5 probes at $R = 0.5$ m and 3 probes at $R = 1$ m, where the calibration error dynamic range is up to $\pm 0.5$ dB in amplitude and $\pm 3.4^o$ in phase, respectively.

## REFERENCES

[1] T. Takahashi, Y. Konishi, and I. Chiba, "A novel amplitude-only measurement method to determine element fields in phased arrays," *IEEE Transactions on Antennas and Propagation*, vol. 60, no. 7, pp. 3222–3230, July 2012.

[2] R. Long, J. Ouyang, F. Yang, W. Han, and L. Zhou, "Multi-element phased array calibration method by solving linear equations," *IEEE Transactions on Antennas and Propagation*, vol. 65, no. 6, pp. 2931–2939, June 2017.

[3] Z. Wang, F. Zhang, H. Gao, O. Franek, G. F. Pedersen, and W. Fan, "Over-the-air array calibration of mmwave phased array in beam-steering mode based on measured complex signals," *IEEE Transactions on Antennas and Propagation*, pp. 1–1, 2021.

[4] F. Zhang, W. Fan, Z. Wang, Y. Zhang, and G. F. Pedersen, "Improved over-the-air phased array calibration based on measured complex array signals," *IEEE Antennas and Wireless Propagation Letters*, vol. 18, no. 6, pp. 1174–1178, June 2019.

[5] F. Zhang, H. Gao, Z. Wang, and W. Fan, "An improved complex signal based calibration method for beam-steering phased array," *IEEE Antennas and Wireless Propagation Letters*, pp. 1–1, 2021.

[6] L. Kuai, J. Chen, Z. H. Jiang, C. Yu, C. Guo, Y. Yu, H. Zhou, and W. Hong, "A n260 band 64 channel millimeter wave full-digital multi-beam array for 5g massive mimo applications," *IEEE Access*, vol. 8, pp. 47 640–47 653, 2020.

[7] A. E. Sayers, W. M. Dorsey, K. W. O'Haver, and J. A. Valenzi, "Planar near-field measurement of digital phased arrays using near-field scan plane reconstruction," *IEEE Transactions on Antennas and Propagation*, vol. 60, no. 6, pp. 2711–2718, 2012.

[8] H.-T. Chou, J. W. Liu, and W.-J. Liao, "Fast phased array antenna calibration incorporating with a far-field radiation measurement system," in *2019 13th European Conference on Antennas and Propagation (EuCAP)*, 2019, pp. 1–4.

[9] Y. Zhang, Z. Wang, X. Sun, Z. Qiao, W. Fan, and J. Miao, "Design and implementation of a wideband dual-polarized plane wave generator with tapered feeding nonuniform array," *IEEE Antennas and Wireless Propagation Letters*, vol. 19, no. 11, pp. 1988–1992, 2020.

[10] L. Wegrowicz and R. Pokuls, "Inverse problem approach to array diagnostics," in *Antennas and Propagation Society Symposium 1991 Digest*, 1991, pp. 1292–1295 vol.2.

[11] W. Fan, F. Zhang, Z. Wang, O. K. Jensen, and G. F. Pedersen, "On angular sampling intervals for reconstructing wideband channel spatial profiles in directional scanning measurements," *IEEE Transactions on Vehicular Technology*, vol. 69, no. 11, pp. 13 910–13 915, 2020.